

# We are IntechOpen, the world's leading publisher of Open Access books Built by scientists, for scientists

6,900

Open access books available

186,000

International authors and editors

200M

Downloads

Our authors are among the

154

Countries delivered to

TOP 1%

most cited scientists

12.2%

Contributors from top 500 universities



WEB OF SCIENCE™

Selection of our books indexed in the Book Citation Index  
in Web of Science™ Core Collection (BKCI)

Interested in publishing with us?  
Contact [book.department@intechopen.com](mailto:book.department@intechopen.com)

Numbers displayed above are based on latest data collected.  
For more information visit [www.intechopen.com](http://www.intechopen.com)



# Fracture Mechanics Analysis of Fretting Fatigue Considering Small Crack Effects, Mixed Mode, and Mean Stress Effect

Kunio Asai

Additional information is available at the end of the chapter

<http://dx.doi.org/10.5772/51463>

## 1. Introduction

Like sharp-notch fatigue, fretting fatigue strength is mostly determined by whether small cracks propagate, which originate at the local high stress area. Hence, applying fracture mechanics is expected to be effective in evaluating fretting strength (Asai, 2010; Attia, 2005; Edward, 1984; Kondo et al., 2004; Makino et al., 2000; Nicholas et al., 2003). In these methods, the fretting fatigue limit is predicted by evaluating whether the stress intensity factor range  $\Delta K$  is greater than its threshold value  $\Delta K_{th}$ . Kondo (Kondo et al., 2004) developed a model for evaluating micro-crack propagation, which is shown in Fig. 1. In this model, when  $\Delta K$  is lower than  $\Delta K_{th}$  at a certain crack depth, the crack is thought to stop propagation and to remain as a non-propagating crack (O). On the other hand, when  $\Delta K$  is larger than  $\Delta K_{th}$  along the entire crack length, it is thought to propagate to failure. The objective of this study is to evaluate fretting fatigue strength quantitatively using this model under various test conditions including different material strengths, contact pressure, and mean stress by overcoming the following difficulties.

The following two major difficulties need to be addressed when quantitatively applying the micro-crack propagation model.

1. Small crack and mean stress effects on  $\Delta K_{th}$ ,
2. Mixed modes of tensile and shear  $\Delta K$ .

Regarding the small crack effects on  $\Delta K_{th}$ , El Haddad (El Haddad et al., 1979) proposed the correlation factor,  $a_0$ , for the crack length,  $a$ , and the threshold of a long crack,  $\Delta K_{th, l}$ , as expressed in Eq. (1),

$$\Delta K_{th} = \Delta K_{th, l} \sqrt{a / (a + a_0)}. \quad (1)$$

The empirical rule proposed by Murakami (Murakami & Endo, 1986) is also well known, where  $\Delta K_{th}$  is proportional to one-third power of the square root of the micro-crack surface area, equivalent to crack length. Although these approaches are effective in estimating  $\Delta K_{th}$  for micro cracks, there are few data available for the mean stress effects on micro-crack  $\Delta K_{th}$  (Usami & Shida, 1979), especially under a high negative stress ratio ( $R$ ), which is indispensable in evaluating the fretting fatigue strength.

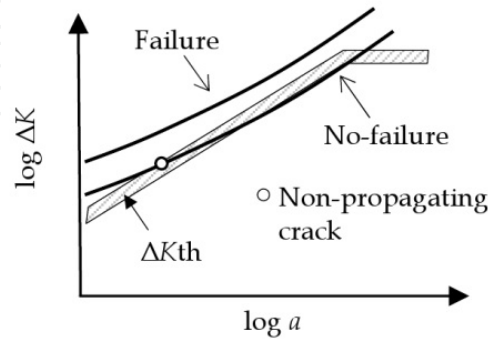


**Figure 1.** Schematic of small-crack propagation model at fretting fatigue

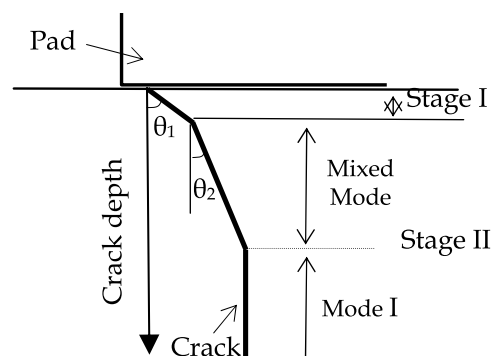


**Figure 2.** Schematic view of fretting crack propagation

Mixed modes of tensile and shear  $\Delta K$  should be considered because most fretting fatigue cracks incline under multi-axial stress fields caused by the contact pressure and tangential force (Lamacq et al., 1996; Qian & Fatemi, 1996; Zhang & Fatemi, 2010). According to Mutoh (Mutoh, 1997), the crack path of fretting fatigue is classified into two stages, as shown in Fig. 2. Stage I is an initial crack stage where a crack inclines greatly against the normal direction, and stage II is where a crack is thought to propagate in the direction perpendicular to the maximum principal stress amplitude. As many researchers state (Dubourg & Lamacq, 2000; Faanes, 1995; Mutoh & Xu, 2003), maximum tangential stress theory is considered to be effective for expressing the crack propagation in stage II; hence, one problem is how to model its propagation in stage I. To solve this problem, Pook's failure mechanism map (Pook, 1985) in the  $\Delta K_I - \Delta K_{II}$  plane is informative for separating crack propagation patterns into shear and tensile modes. Although it was proposed to define equivalent stress intensity factors, such as  $\sqrt{\Delta K_I^2 + \Delta K_{II}^2}$  based on the strain energy release rate, and  $(\Delta K_I^4 + 8\Delta K_{II}^4)^{1/4}$  from Tanaka (Tanaka, 1974), there seems to be no unified model applicable to various test results (Hannes & Alfredsson, 2012). Summarizing the studies on mixed modes, what makes it

difficult to explain the crack propagation in stage I are the difficulties in experimentally obtaining the mode II thresholds (Murakami et al., 2002) and quantitatively estimating the actual  $\Delta K_{II}$  considering the crack surface friction effects (Bold et al., 1992). However, from the standpoint of practical use, it is thought useful to apply the maximum tangential stress theory in stage I if its estimation is satisfactorily accurate.

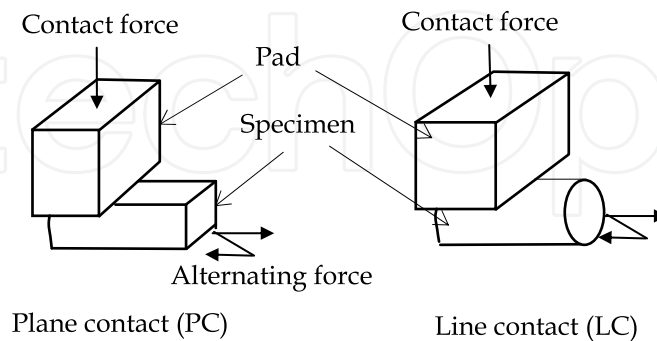


**Figure 3.** Schematic view of fretting fatigue tests

In this study, fretting fatigue tests under different contact conditions; plane-contact (PC) and line-contact (LC), shown in Fig. 3, were carried out using two 12% Cr steel samples with different static strengths and the effects of the material strength and mean stress were investigated. Fretting fatigue strength was evaluated quantitatively by applying the micro-crack propagation model under various test conditions while considering the above-mentioned difficulties. The practical effectiveness is discussed in applying the maximum tangential stress theory in stage I by obtaining non-propagating crack lengths of run-out specimens and  $\Delta K_{th}$  from fretting pre-cracks under various R, including negative mean stress.

## 2. Fretting test method

The test materials were two 12% Cr steel samples (A and B) that had different static strengths, as shown in Table 1. Tensile and 0.2% yield strengths of sample B were approximately 40% higher than those of sample A. Figure 4 shows the shapes of the test specimens and a contact pad. Two kinds of tests were undertaken using rectangular-cross-section specimens (5 mm × 5 mm) for PC conditions and circular-cross-section specimens (8 mm in diameter) for LC conditions. Sample A was used for the contact pad. Heat treatments were applied to the specimens at 600°C × 4 h to relieve the residual stress caused by machining.

After first applying an axial mean load, the contact force was applied using cramping bolts, and axial alternative loads were then applied. The contact force was measured and adjusted by the cylindrical load cell with an uncertainty of 5% to the target value during the tests. Contact pressure was 80 MPa for PC conditions, and LC loads were 60, 150, 300, and 450 N/mm, which respectively corresponded to 584, 923, 1306, and 1569 MPa of the average elastic contact pressure calculated from Hertz's formula. Mean stresses were 0 and 400 MPa for all test cases and -100 MPa for PC conditions of sample A. Tests were carried out using an electro-magnetic-resonance machine in air at ambient temperature. The frequencies were about 125 Hz for LC and about 110 Hz for PC, which were determined by the stiffness of the specimens and the machine.

	0.2% proof stress	Tensile strength	Elongation (%)	Reduction of area	Vickers hardness
Sample A	610	745	26.3	65.5	238
Sample B	842	1037	15.4	51.0	329

**Table 1.** Mechanical properties of materials

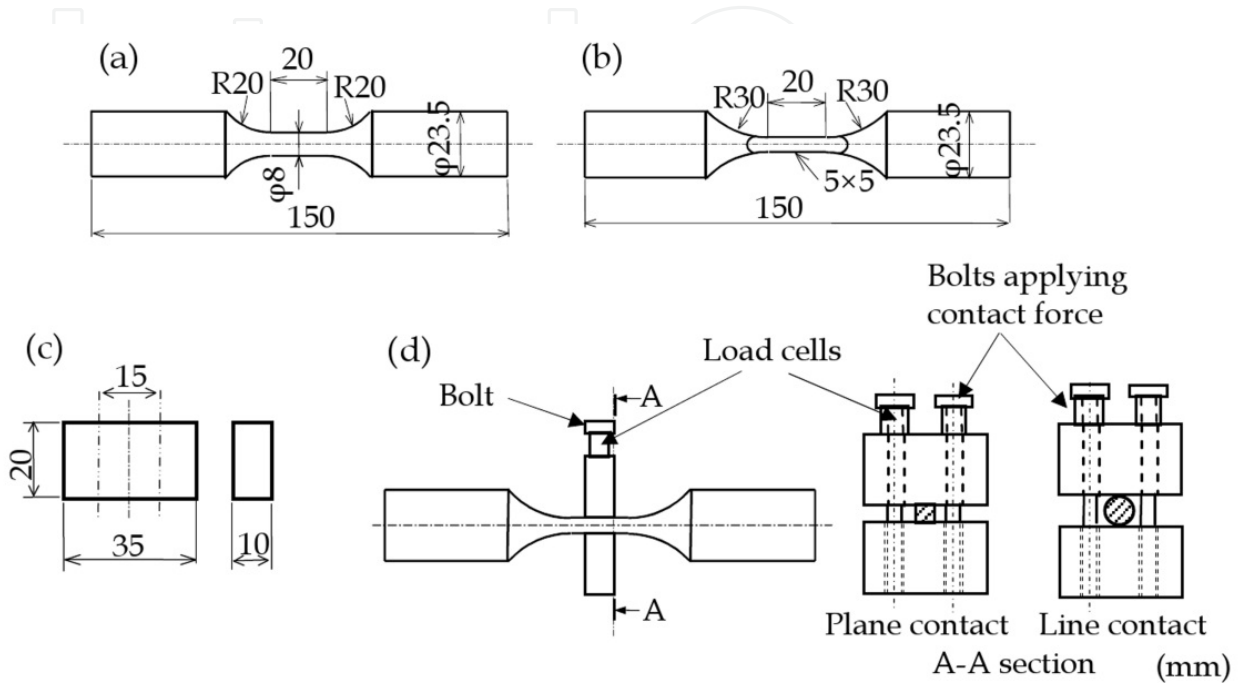


**Figure 4.** Shapes of specimens and test apparatus: (a) specimen for LC tests, (b) specimen for PC tests, (c) contact pad, and (d) test apparatus

Plain fatigue tests were also carried out without contact pads using run-out fretting specimens at  $2 \times 10^7$  cycles, and the size of fretting non-propagating cracks, which were the cause of plain fatigue fracture in most cases, were investigated. In addition to the crack length, the plain fatigue tests were aimed at obtaining  $\Delta K_{th}$  from the fretting pre-crack under constant R, -3, -1, 0, 0.5, by increasing the applied stress step by step until the specimens broke. In these tests, the number of run-out cycles was defined as  $10^7$  and maximum and minimum applied nominal stresses were not to exceed 0.2% yield strength. The crack-profile path from the initial point was also measured at the fracture surface by using a laser microscope to analyze the behavior of the crack propagation. When the specimen did not break from the fretting non-propagating crack, its depth was measured by polishing the crack surface until it disappeared.

### 3. Fretting fatigue test results

#### 3.1. Fretting fatigue strength

Figure 5 shows the stress amplitude  $\sigma_a$  against the number of cycles (S-N) diagrams for PC and LC conditions. Figure 6 shows the effect of the contact pressure on fretting fatigue

strength when mean stresses  $\sigma_m$  were 0 and 400 MPa, indicating failure- and non-failure-stress amplitudes at  $2 \times 10^7$  cycles, respectively. The fatigue limits for LC conditions decreased as the contact pressure increased and minimized at a certain contact pressure. The minimum strength pressure, *MSP*, when fretting fatigue strength minimized, depended on the material strength, i.e., *MSP* of sample B (higher static strength) was higher than that of sample A. The average Hertz's contact pressure at *MSP* almost corresponded to about 1.5 times 0.2% proof stress  $\sigma_{0.2}$  for both samples A and B. Under PC, sample B exhibited 10-25% higher fretting-fatigue strength than sample A. On the other hand, the minimum strengths of samples A and B differed little (about 5%) under LC conditions; this tells us that a high-static-strength material does not necessarily improve the fretting fatigue strength when local high contact pressure arises. Fretting fatigue strength depended on the mean stress in a high contact pressure region; the strength over *MSP* increased more drastically at  $\sigma_m=0$  MPa than that at  $\sigma_m=400$  MPa.

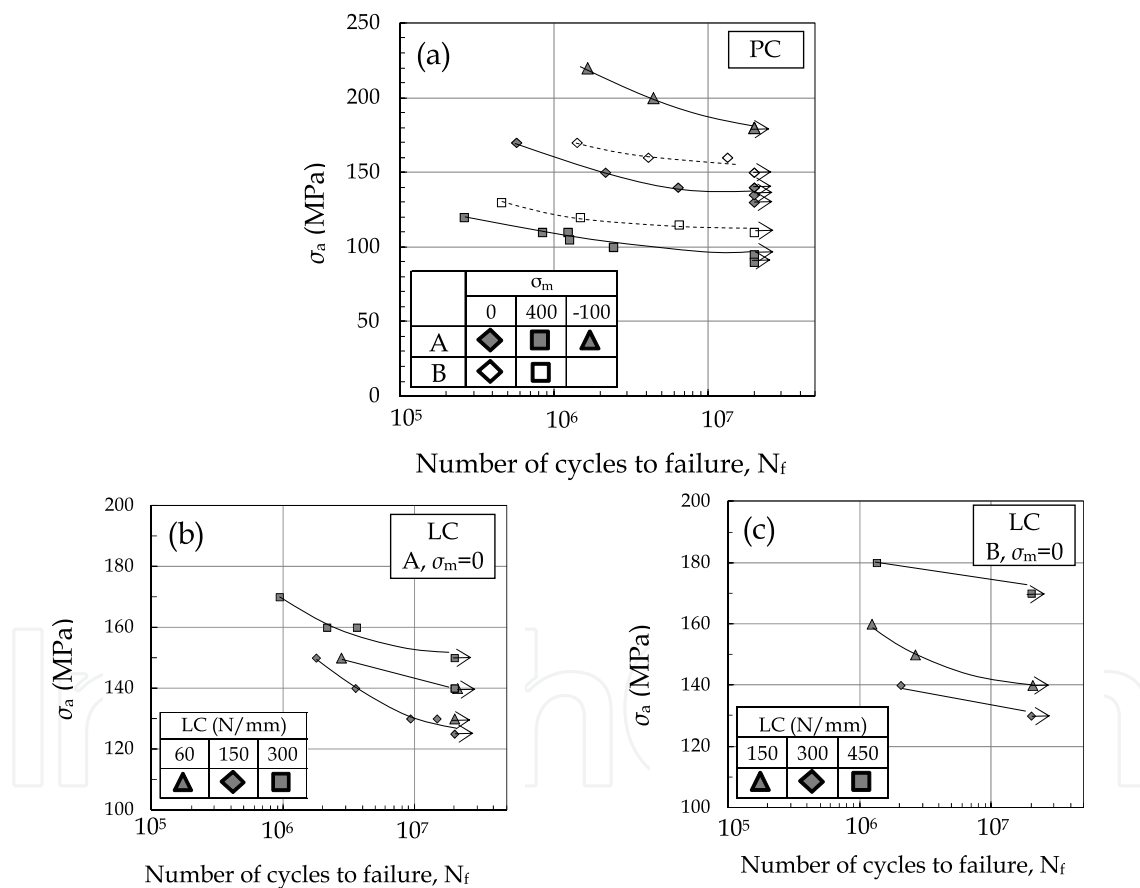


**Figure 5.** S-N diagram of fretting tests: (a) PC, (b) LC for sample A, and (c) LC for sample B

Figure 7 shows an observed contact surface near the contact edge under LC conditions at 150 N/mm-pressure. The crack edge was located about 0.12 mm inside the contact edge. The width of the wear region was about 0.5 mm, greater than the elastic contact width calculated from Hertz's formula (about 0.16 mm). This was caused by plastic deformation at the contact edge under high local pressure.

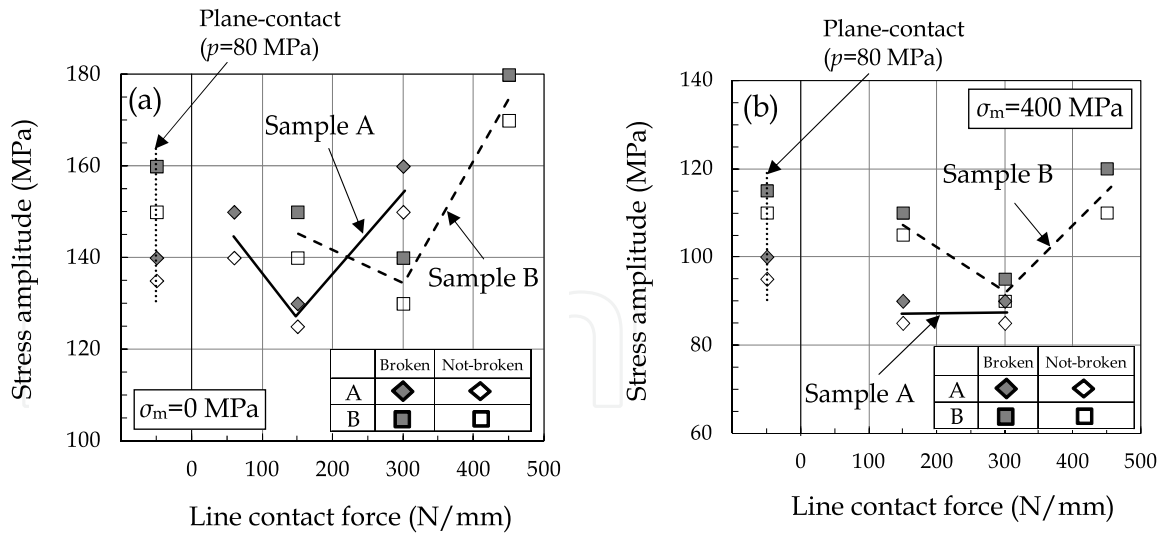


**Figure 6.** Effect of contact pressure on fretting fatigue strength at mean stress, (a) 0 MPa, and (b) 400 MPa. (Open: not broken; closed: broken in less than  $2 \times 10^7$  cycles)

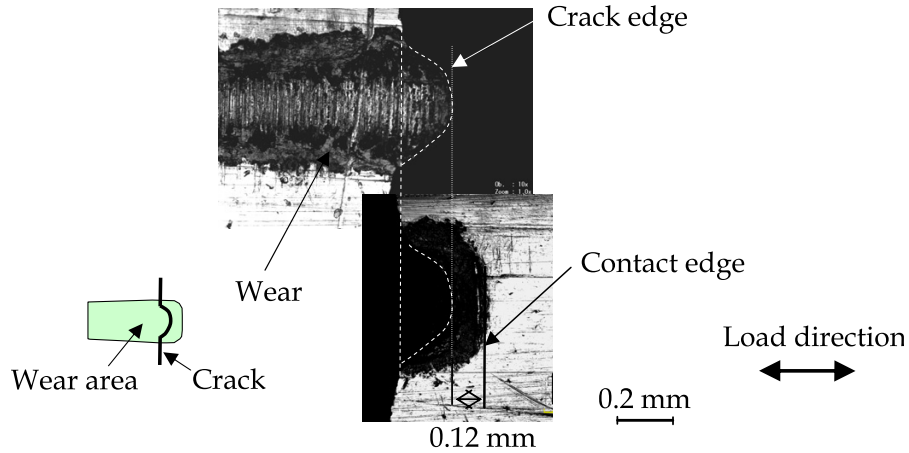


**Figure 7.** Side view around contact edge of failure specimen. (Sample A: LC, 150 N/mm,  $\sigma_m = 0$  MPa,  $\sigma_a = 130$  MPa,  $N_f = 9.23 \times 10^6$ )

### 3.2. Dimensions of non-propagating cracks

Figure 8(a) shows an example of a non-propagating crack at the fracture surface. Its depth  $a$  and surface length  $l$ , projected in the plane perpendicular to the axial direction, were obtained from the fracture surfaces. The value of  $a/l$  was almost 0.15, as shown in Fig. 8(b). The relationship between non-propagating crack length  $a_{eq}$  and stress amplitude is summarized in Fig. 9, where equivalent crack length  $a_{eq}$  was calculated from Eq. (2).

$$a_{eq} = a/Q, \quad Q = 1 + 4.593(a/l)^{1.65}. \quad (2)$$

The value of  $a_{eq}$  corresponds to half the center crack length of the infinite plate under uniform stress field. Figure 9 suggests the following three characteristics:

- The value of  $a_{eq}$  for sample B (higher static strength) is smaller than that of sample A on the same  $\sigma_a$  under PC.

- Higher mean stress leads to smaller  $a_{eq}$  at the fatigue limit under PC
- Under LC, the relations of  $\sigma_a - a_{eq}$  are almost the same under various contact pressures and mean stresses

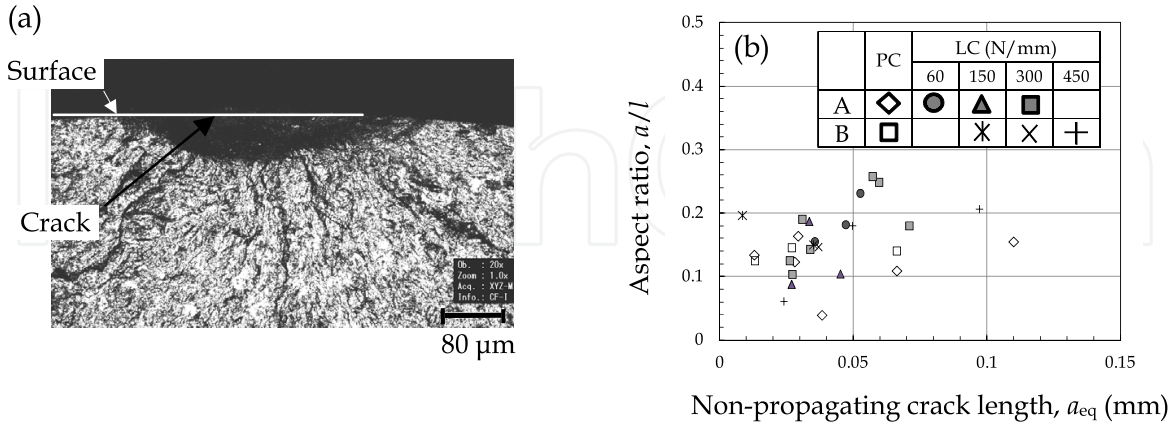


Figure 8. (a) Example of non-propagating crack and (b) aspect ratio of non-propagating cracks

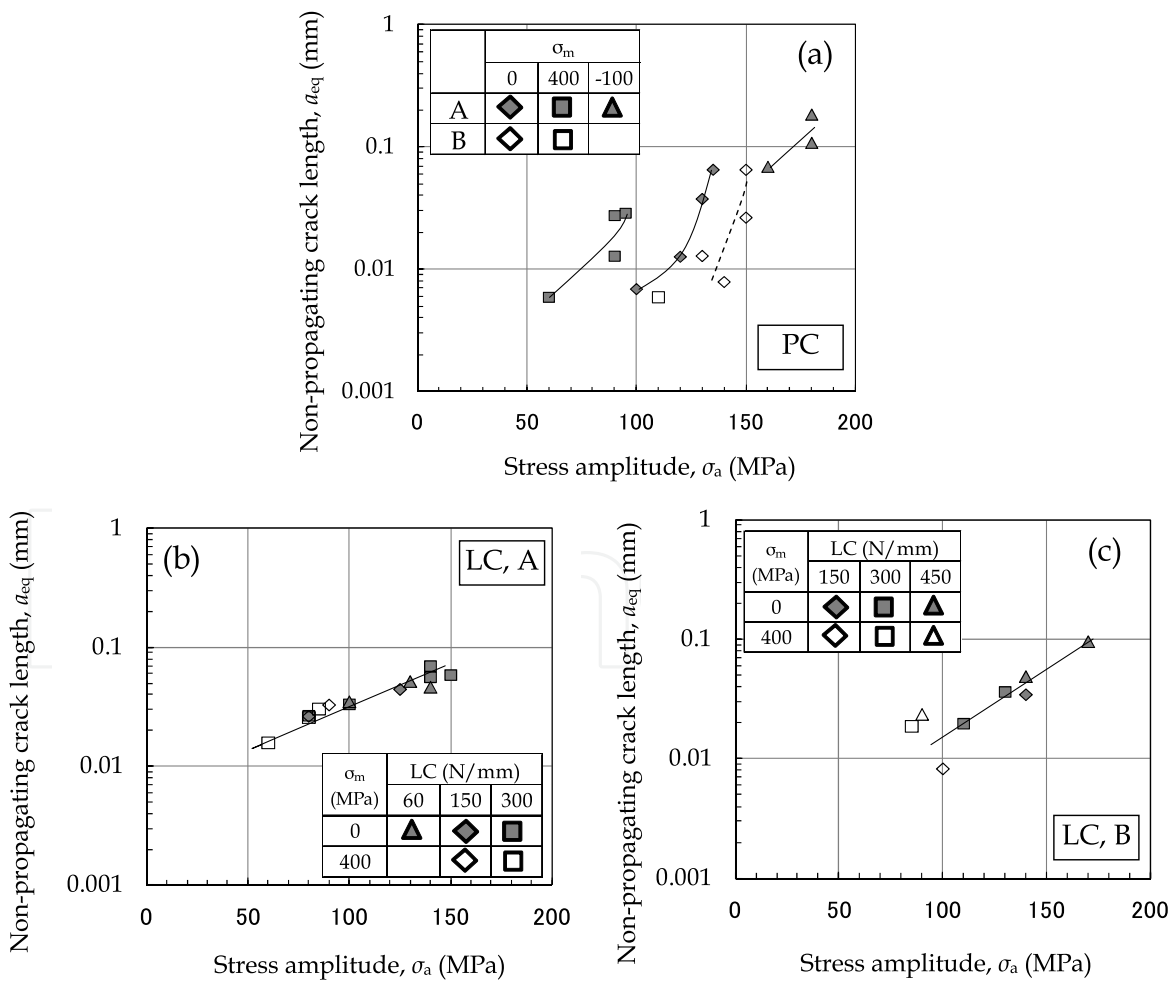


Figure 9. Non-propagating crack depth obtained from fretting fatigue tests: (a) PC, (b) LC (sample A), and (c) LC (sample B)

### 3.3. Profile path of crack propagation

Figure 10 shows profile paths of crack propagation from the initial crack measured using a laser-microscope, where the stress amplitude is shown in parentheses for each case. The angle of crack inclination against the normal direction was about 50-70° in stage I and about 20° at the mixed mode region in stage II, as also shown in Fig. 10.

Non-propagating cracks under PC conditions were almost all located in stage II except one case (sample B at 400 MPa-mean stress) when no profile data were obtained because the run-out specimen was not fractured from the fretting pre-crack. On the other hand, under LC conditions, all non-propagating cracks were located near the boundary between stages I and II. The boundary crack depth between stages I and II,  $d_1$ , depended on the mean stress, contact pressure, and material strength. The following explains why this occurred.

- The values of  $d_1$  of sample B (higher static strength) were smaller than those of sample A under the same test conditions.
- The values of  $d_1$  under PC condition were smaller than those under LC conditions at the same mean stress.
- 400 MPa-mean stress led to lower  $d_1$  than 0 MPa-mean stress under LC conditions.
- When mean stress was -100 MPa in the PC condition,  $d_1$  was extremely small (less than 5  $\mu\text{m}$ ).

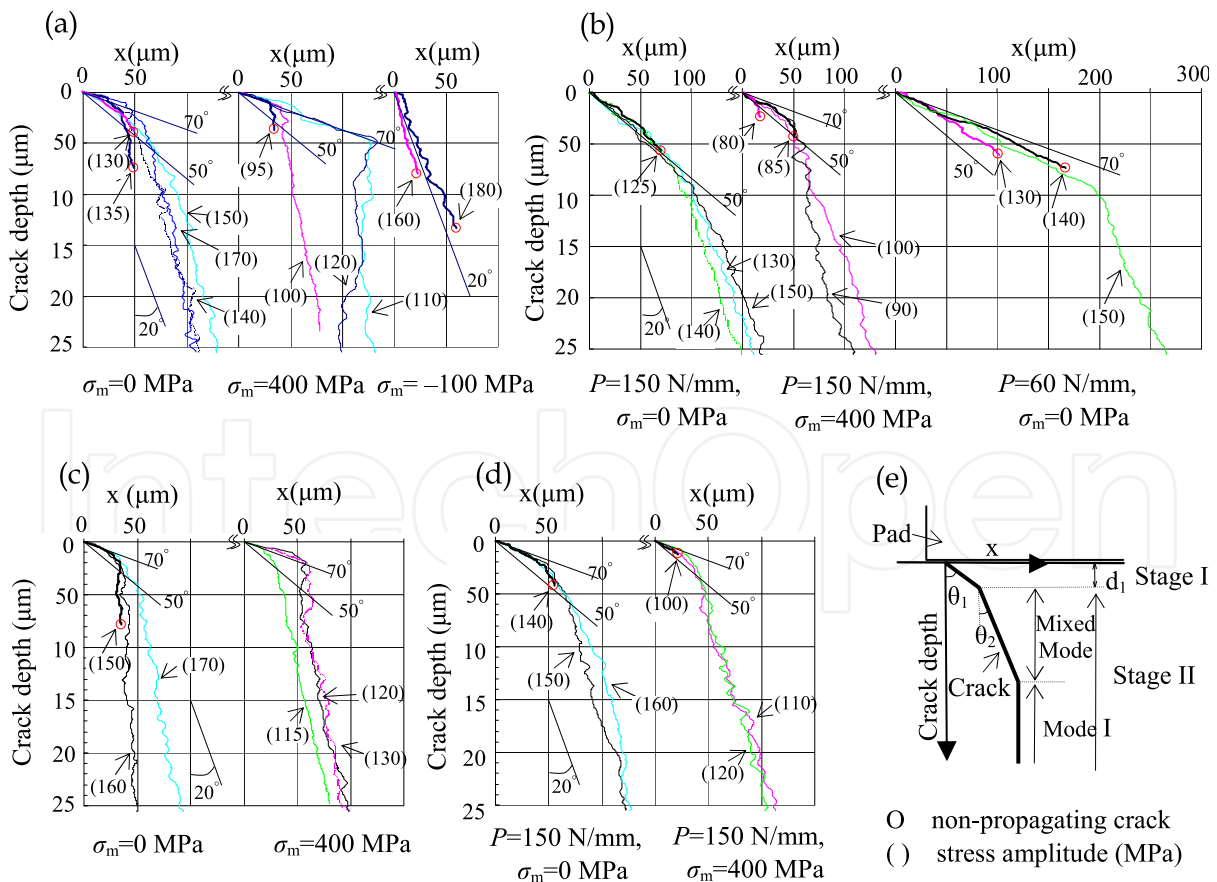


**Figure 10.** Non-propagating and propagating crack profiles obtained from fretting fatigue tests: (a) PC (sample A), (b) LC (sample A), (c) PC (sample B), (d) LC (sample B), and (e) schematic view of fretting crack

These results regarding  $d_1$  and its inclined angles can be described by considering crack propagation under mixed modes in stage I, but the details are to be discussed in future work. The objective with this study was to quantitatively evaluate the micro-crack propagation in stages I and II by applying the maximum tangential stress theory.

## 4. Discussions

### 4.1. Analysis condition for calculating stress intensity factor

The relationship between crack depth and the stress intensity factor was calculated by carrying out three-dimensional elastic Finite Element (FE) analysis. Figure 11 shows the analysis models under PC and LC conditions where an inclined elliptical surface crack was introduced. The aspect ratio (the ratio of crack depth to surface length) was 0.15 determined from the results shown in Fig. 8(b). The crack depths were 0.03, 0.06, 0.1, and 0.2 mm ( $a_{eq}=0.025, 0.05, 0.083, \text{ and } 0.17$  mm) and the oblique angle against the normal direction,  $\alpha$ , was  $20^\circ$  on the basis of the test results in the mixed mode region of stage II. Furthermore, to investigate the effect of  $\alpha$  for a small crack, analysis was done when  $\alpha=0, 20, 50, 70^\circ$  at  $a_{eq}=0.025, \text{ and } 0.05$  mm. A crack was introduced 0.1 mm inside the contact edge to prevent the edge effect in contact analysis and to be consistent with the test results shown in Fig. 7. The friction coefficient was 0.8, determined from gross slip tests. Calculated accuracy was compared with the analytical solution through analysis without contact.

The stress intensity factor ranges  $\Delta K_I$  and  $\Delta K_{II}$  were calculated using the extrapolation method of stress distribution from the deepest point of the crack. By substituting  $\Delta K_I$  and  $\Delta K_{II}$  into Eq. (3), tensile  $\Delta K_\theta$  and shear  $\Delta K_\tau$  were obtained in the local coordinate system at any evaluation angle  $\theta$ .

$$\begin{aligned}\Delta K_\theta &= \Delta K_I \left( \frac{3}{4} \cos \frac{\theta}{2} + \frac{1}{4} \cos \frac{3\theta}{2} \right) + \Delta K_{II} \left( -\frac{3}{4} \sin \frac{\theta}{2} - \frac{3}{4} \sin \frac{3\theta}{2} \right) \\ \Delta K_\tau &= \Delta K_I \left( \frac{1}{4} \sin \frac{\theta}{2} + \frac{1}{4} \sin \frac{3\theta}{2} \right) + \Delta K_{II} \left( \frac{1}{4} \cos \frac{\theta}{2} + \frac{3}{4} \cos \frac{3\theta}{2} \right)\end{aligned}\quad (3)$$

Alternating axial loads over one cycle were applied after applying the mean axial load and the contact force. The stress intensity factor range  $\Delta K_\theta$  is the difference of  $K_\theta$  at the maximum and minimum loads, and the mean value  $K_{\theta, \text{mean}}$  is the average of  $K_\theta$  at these loads.

Elasto-plastic analysis was also done under LC conditions to investigate the effects of local plastic deformation using the non-crack model whose minimum mesh size was  $10 \mu\text{m}$  at the contact edge. Cyclic stress-strain test data were used in the calculation to consider the cyclic softening effects of test materials, where the cyclic 0.2% yield strengths were about 82% of the static ones for both samples A and B. The alternating force was applied after applying the mean stress and contact pressure in three cycles to obtain the convergence stress distribution.

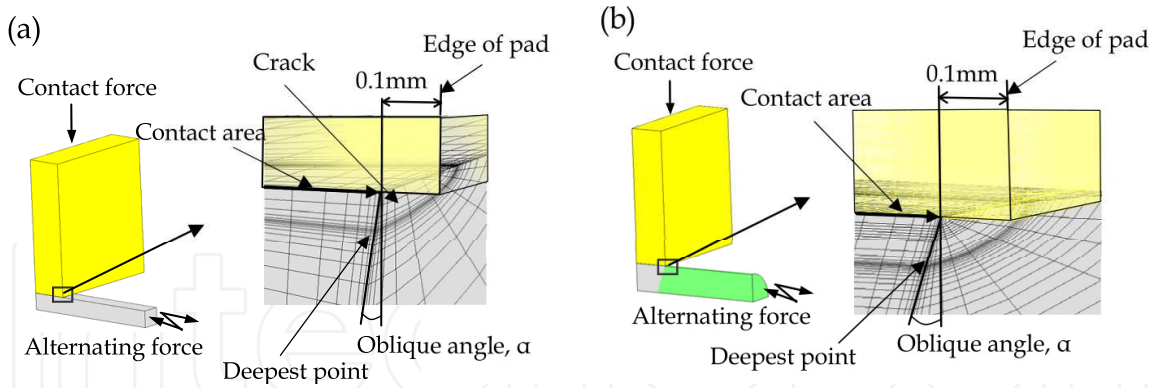


**Figure 11.** FE analysis model with crack of (a) PC and (b) LC (1/8 symmetry)

### 4.2. Analysis results on stress intensity factor

Figure 12 shows the variation of  $\Delta K_\theta$  and  $\Delta K_\tau$  against  $\beta$ , defined as the angle of the evaluation direction against the normal direction, when a crack was 0.03 mm deep under PC conditions ( $p=80$  MPa,  $\sigma_a=100$  MPa, and  $\sigma_m=0$  MPa). The angle  $\beta$  is  $20^\circ$  when  $\Delta K_\theta$  maximizes, which slightly depends on the crack  $\alpha$ . This angle of  $\beta$  corresponds well to the inclined crack angle confirmed by tests at the mixed mode in stage II, as shown in Fig. 10. This supports the maximum tangential stress theory that the fretting fatigue crack propagates in a direction perpendicular to the maximum principal stress amplitude in stage II. When  $\beta$  is  $50\text{--}70^\circ$ , corresponding to the inclined angle of the initial crack in stage I,  $\Delta K_\tau$  is not zero. This suggests that both  $\Delta K_\tau$  and  $\Delta K_\theta$  affect crack propagation in stage I, unlike in stage II. As shown in Fig. 12(b),  $K_{\theta, \text{mean}}$  is negative, and its absolute value decreases with  $\beta$  when  $\beta$  is less than about  $60^\circ$ .

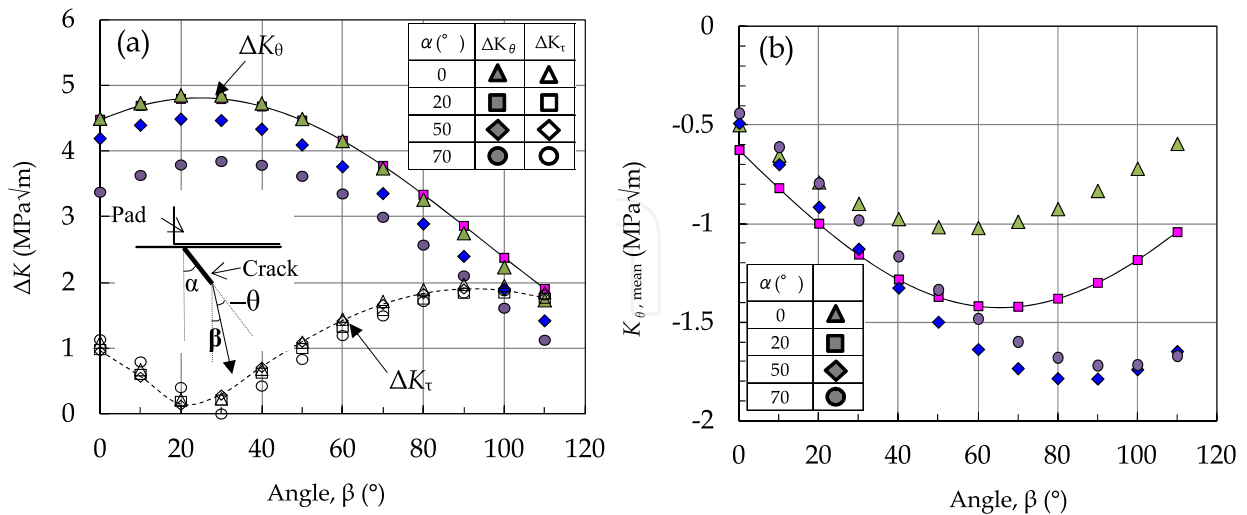


**Figure 12.** Calculated stress intensity factors for oblique cracks as function of  $\beta$ : (a)  $\Delta K_\theta$  and  $\Delta K_\tau$ , and (b) mean value of  $K_\theta$  (PC,  $p=80$  MPa,  $\sigma_m=0$  MPa,  $\sigma_a=100$  MPa,  $a_{\text{eq}}=0.025$  mm)

Next, Figs. 13(a) and (b) show the relationships between  $a_{\text{eq}}$  and  $\Delta K_{\theta\text{max}}$  and mean value  $K_{\theta\text{max, mean}}$  when  $\sigma_m=0$  MPa and  $\sigma_a=100$  MPa. The value of  $\Delta K_{\theta\text{max}}$  is the maximum value of

$\Delta K_{\theta}$  with the variation of  $\beta$  and  $K_{\theta_{\max, \text{mean}}}$  is the mean  $K_{\theta}$  when  $\Delta K_{\theta}$  is  $\Delta K_{\theta_{\max}}$ . When the crack is short,  $\Delta K_{\theta_{\max}}$  is strongly affected by the contact and, as the crack grows, it asymptotically reaches the value calculated under the uniform stress distribution without fretting effects.  $\Delta K_{\theta_{\max}}$  at  $\alpha=0^{\circ}$  and  $20^{\circ}$  without contact were confirmed to coincide within 3% of error with the solution of the Raju-Newman equation (Raju & Newman, 1981). The values of  $\Delta K$  at  $\alpha=70^{\circ}$  were found to be about 30% smaller than those at  $\alpha=0^{\circ}$  under both contact and non-contact conditions. The absolute value of  $K_{\theta_{\max, \text{mean}}}$  decreases as a crack grows, as shown in Fig. 13(b). This is because the compression stress caused by the contact force decreases as the distance from the surface increases.

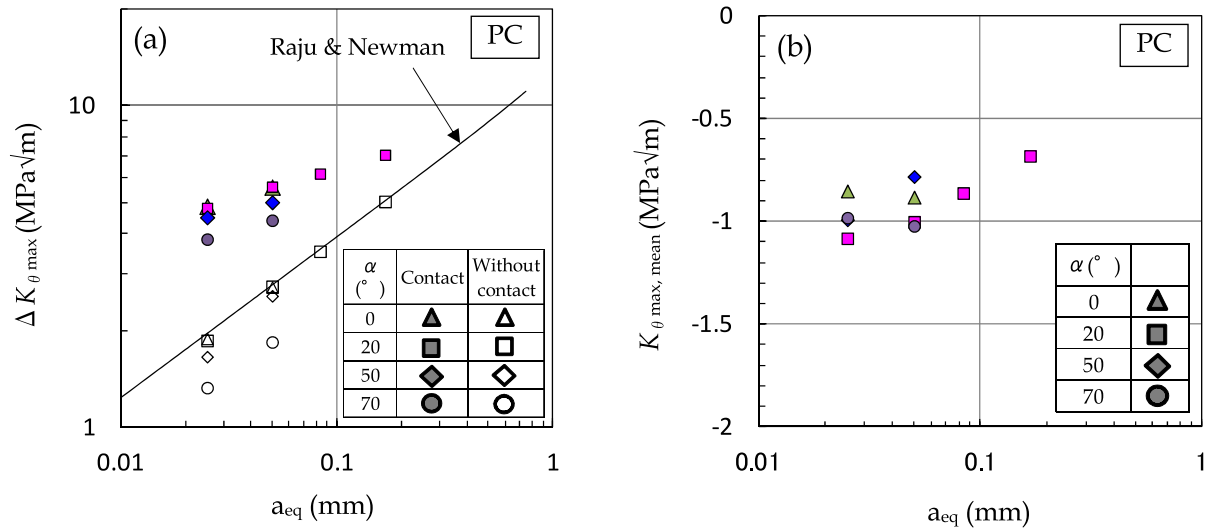


**Figure 13.** Relationship between  $a_{\text{eq}}$  and (a)  $\Delta K_{\theta_{\max}}$  and (b)  $K_{\theta_{\max, \text{mean}}}$  calculated using FE analysis (PC,  $p=80$  MPa,  $\sigma_m=0$  MPa,  $\sigma_a=100$  MPa)

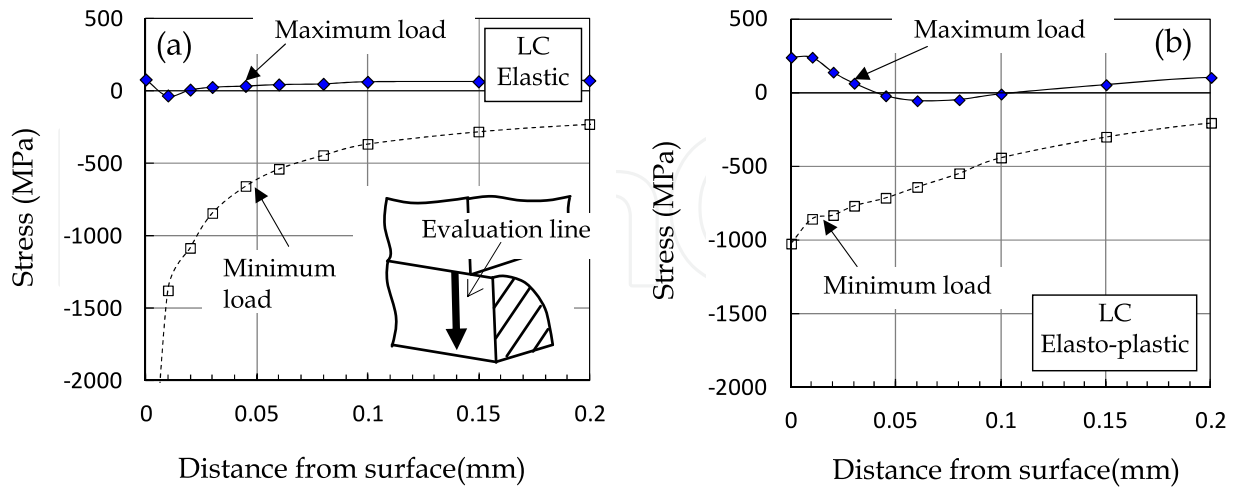


**Figure 14.** Axial stress distribution from the surface with non-crack model calculated by (a) elastic and (b) elasto-plastic analyses (LC,  $P=150$  N/mm,  $\sigma_m=0$  MPa,  $\sigma_a=100$  MPa)

The stress distributions calculated using elastic and elasto-plastic analyses are compared in Fig. 14 for non-crack models under LC conditions for sample A when  $P=150$  N/mm,  $\sigma_m=0$

MPa, and  $\sigma_a=100$  MPa. This figure shows the maximum and minimum axial stress distributions along the line from the surface of the contact edge. While high compressive stress arises when using the elastic analysis, the minimum stress almost saturates when calculated using the elasto-plastic analysis. Using the polynomial approximation of the elasto-plastic stress distributions without a crack,  $\Delta K$  and  $K_{\text{mean}}$  were calculated using the American Society of Mechanical Engineers (ASME) section XI method (ASME, 2001). The values of  $\Delta K$  and  $K_{\text{mean}}$  against  $a_{\text{eq}}$  are shown in Fig. 15, where the solid diamond were calculated by the elastic analysis with a crack at  $\alpha=20^\circ$  using the stress extrapolation method and the dashed lines were calculated from the elasto-plastic analysis using the above-mentioned ASME method. As shown in Fig. 15(a),  $\Delta K$ s are almost the same in two calculations except  $a_{\text{eq}}=0.025$  mm, where local stress is higher from elastic analysis than that from elasto-plastic analysis because the former does not take into account the yield effects. On the other hand,  $K_{\text{mean}}$ s are different from the two analyses, especially when  $a_{\text{eq}}$  is small. Since  $K_{\text{mean}}$  affects  $\Delta K_{\text{th}}$ , it is necessary to evaluate stress redistribution using elasto-plastic analysis considering the actual yield behavior under LC conditions.

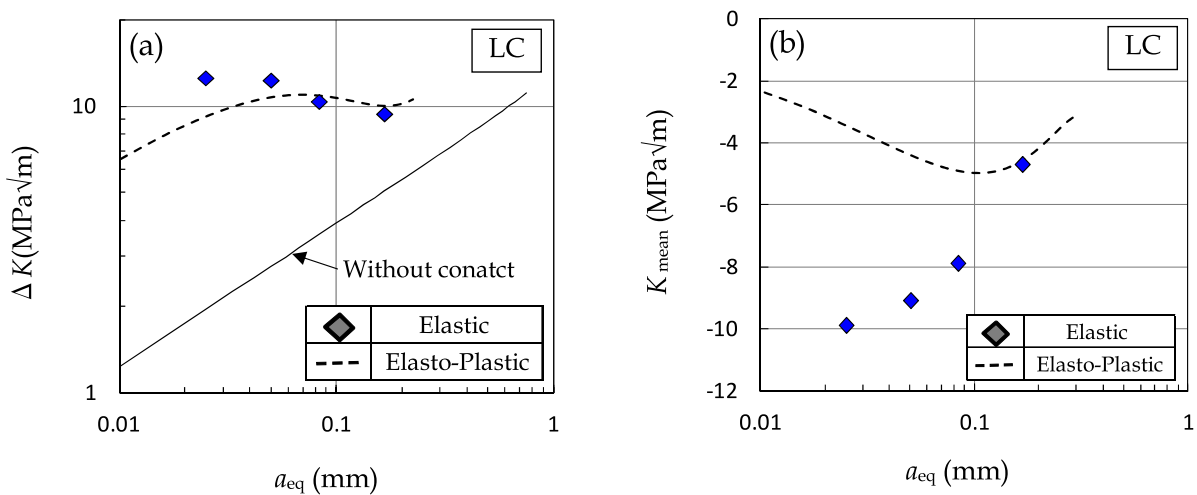


**Figure 15.** Comparison of (a)  $\Delta K$  and (b)  $K_{\text{mean}}$  calculated using elastic analysis with crack model and elasto-plastic analysis with non-crack model (LC,  $P=150$  N/mm,  $\sigma_m=0$  MPa,  $\sigma_a=100$  MPa)

### 4.3. Qualitative evaluation of small crack propagation

Figure 16(a) shows a schematic view of the material strength's effect on  $\Delta K$  under PC. The value of  $\Delta K_{\text{th}}$  in the small crack region increases as the material strengthens:  $\Delta K_{\text{th}}$  of sample B was higher than that of sample A. On the other hand,  $\Delta K$  from the applied stress does not depend on the material strength when the local plastic deformation is ignorable. From this evaluation, the fatigue limit of sample B was higher than that of sample A, which correlates well with the experimental results. Supposing that a crack stops propagating when  $\Delta K$  is smaller than  $\Delta K_{\text{th}}$ , the non-propagating crack depth of sample B is estimated to be smaller than that of sample A under the same stress amplitude. This also agrees well with the experimental results shown in Fig. 9(a).

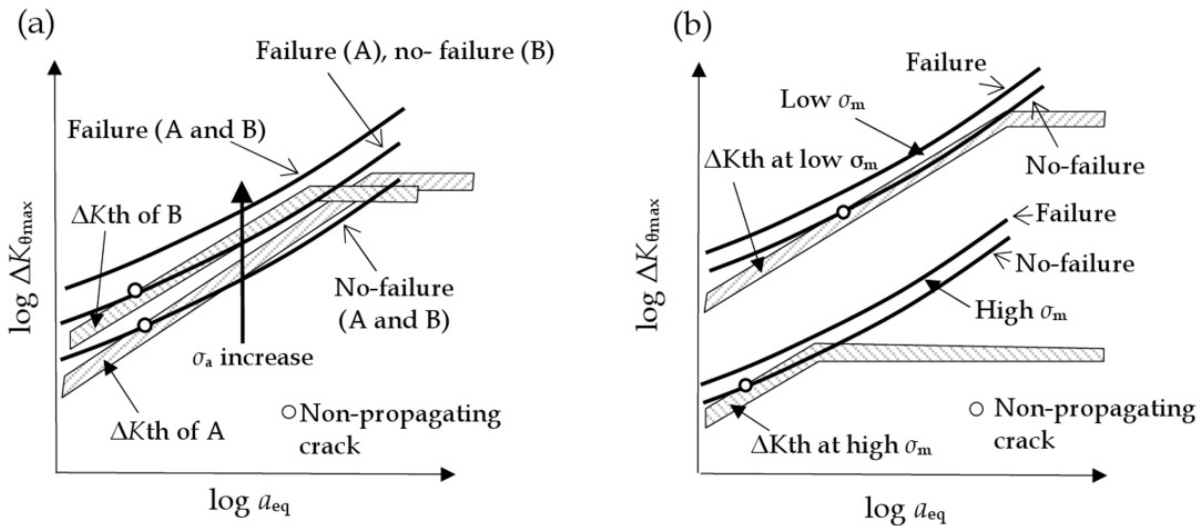


**Figure 16.** Schematics of small-crack propagation model under PC condition on effects of (a) material strength, and (b) mean stress.

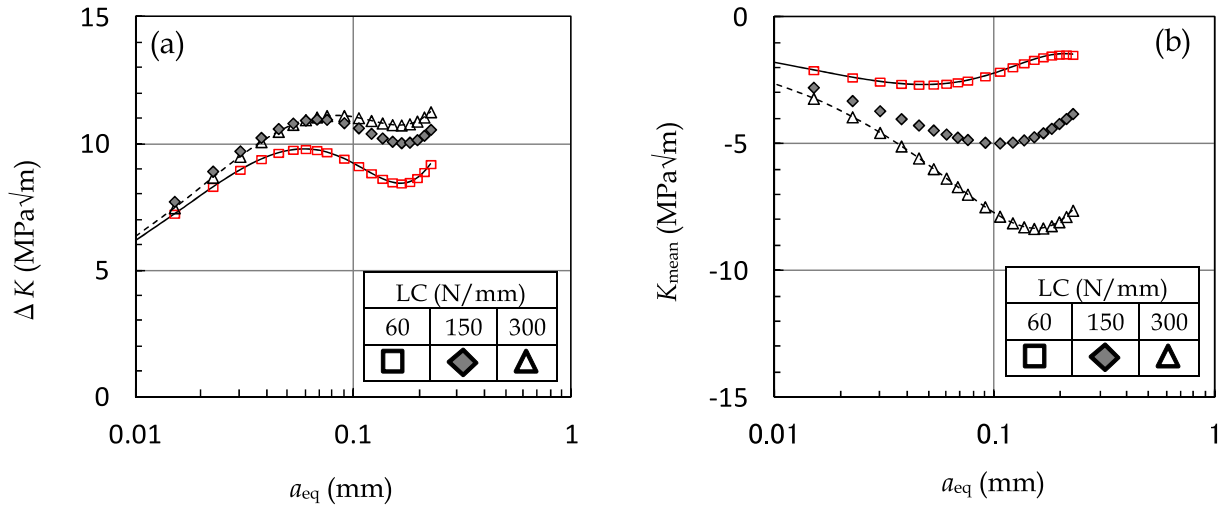


**Figure 17.** Effects of LC pressure on (a)  $\Delta K$ , and (b)  $K_{\text{mean}}$  cacalculated using elasto-plastic analysis with non-crack model (LC,  $\sigma_m=0$  MPa,  $\sigma_a=100$  MPa, sample A)

Figure 16(b) schematically shows the effect of mean stress under PC. Because higher mean stress results in smaller  $\Delta K_{\text{th}}$ , larger  $\sigma_m$  leads to smaller fatigue strength and a smaller non-propagating crack at the fatigue limit from this model. This was also confirmed to correspond well with the results shown in Fig. 9(a).

The fretting fatigue strength minimizes at a certain contact pressure under LC conditions, at 150 N/mm for sample A, as shown in Fig. 6. The relations of  $a_{\text{eq}}-\Delta K$  and  $a_{\text{eq}}-K_{\text{mean}}$  are shown in Fig. 17 for sample A at various contact pressures when  $\sigma_m = 0$  and  $\sigma_a = 100$  MPa. As Fig. 17(a) shows,  $\Delta K$  increases with the contact pressure, but  $\Delta K$ s differ little between 150 and 300 N/mm. On the other hand,  $K_{\text{mean}}$  decreases monotonically with the increase in the LC pressure. This is due to two conflicting effects, the increase in  $\Delta K$  accelerates crack propagation and negative large  $K_{\text{mean}}$  delays its propagation as the contact pressure

increases, that is, 150 N/mm-pressure results in the minimum fretting fatigue strength for sample A.

#### 4.4. $\Delta K_{th}$ from small fretting pre-cracks

Figure 18 shows  $\Delta K_s$  obtained from plain fatigue tests by using fretting pre-crack specimens, where open marks mean non-fracture and closed marks mean fracture. In this figure,  $\Delta K_{th}$ s for long crack are also shown. Estimated  $\Delta K_{th}$ s for small cracks, as boundaries between open and closed marks, were confirmed to depend on the crack length as a slope of 1/3 in the double logarithmic plots under various R. This slope of 1/3 agrees well with Murakami’s empirical rule (Murakami & Endo, 1986). Some data slightly deviated from the approximate line, which was probably caused by inclined pre-crack effects and residual compressive stress due to previous fretting tests.

Threshold values for small cracks are modelled as Eq. (4) using  $\Delta K_{th, 0.1}$ ,  $\Delta K_{th}$  at  $a_{eq}=0.1\text{mm}$  on the 1/3 slope line, and threshold for long cracks,  $\Delta K_{th,l}$ . The variation of  $\Delta K_{th, 0.1}$  is shown in Fig. 19 as a function of R for samples A and B obtained from plain fatigue tests using fretting pre-crack specimens. It was confirmed that the values of  $\Delta K_{th, 0.1}$  for sample B (higher static strength) are higher than those of sample A under all R.

$$\Delta K_{th,s} = \Delta K_{th, 0.1} (a_{eq} / 0.1)^{1/3},$$

$$\Delta K_{th} = \Delta K_{th,s}, \text{ when } \Delta K_{th,s} < \Delta K_{th,l},$$

$$\Delta K_{th} = \Delta K_{th,l}, \text{ when } \Delta K_{th,s} > \Delta K_{th,l}.$$
(4)

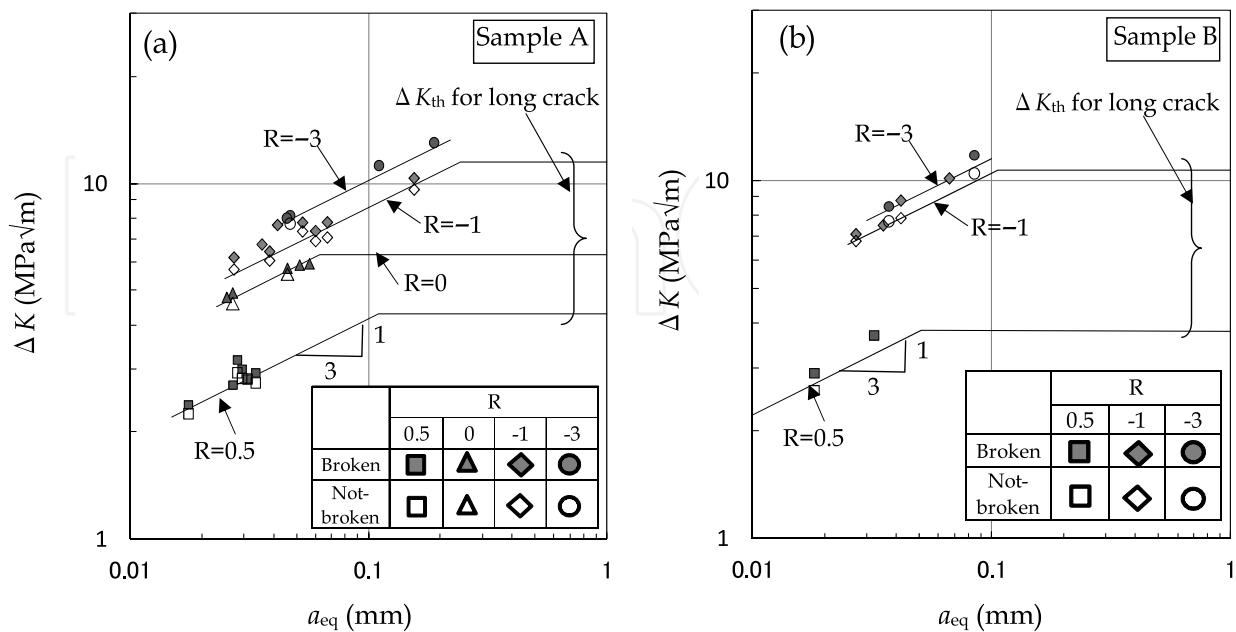


**Figure 18.** The value of  $\Delta K_{th}$  obtained by plain fatigue tests using fretting pre-crack specimens for (a) Sample A and (b) Sample B under various stress ratios

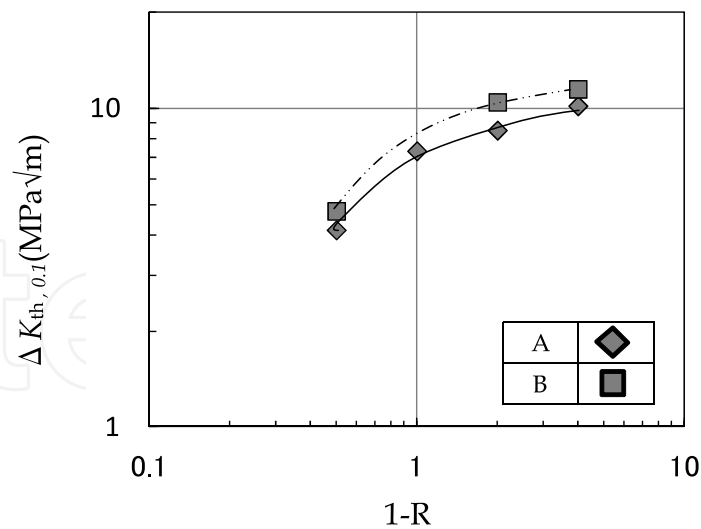


**Figure 19.** The value of  $\Delta K_{th,0.1}$  obtained by tests for steels A and B under various stress ratios as a function of  $1-R$

#### 4.5. Quantitative evaluation of small crack propagation

Micro-crack propagation behavior using the experimental and analytical results under various contact pressures and mean stresses is discussed. Figure 20 shows the evaluation results of fretting fatigue crack propagation under PC conditions when mean stresses are 0, 400, and  $-100$  MPa for sample A and 0, and 400 MPa for sample B. In this figure,  $K_{max}$ ,  $K_{min}$ , and  $\Delta K$  were calculated based on the maximum tangential stress theory at  $\alpha=20^\circ$  using the minimum stress, leading to fracture in the experiments. The value of  $\Delta K_{th}$  was evaluated using Eq. (4) and test results shown in Fig. 19 corresponding to the calculated  $R$ . The analysis results are in good agreement with the test results in all cases since the calculated  $\Delta K$  under the fracture condition is greater than  $\Delta K_{th}$  through almost the entire crack length.

The results are shown in Fig. 21 under LC conditions for sample A evaluated using the micro-crack propagation model when mean stress was 0 and 400 MPa and  $P=60, 150, 300$  N/mm. In this figure,  $K_{max}$ ,  $K_{min}$ , and  $\Delta K$  were calculated using the ASME method with elasto-plastic stress distribution without crack, as discussed in Section 4.2, under minimum stress leading to fracture. The analysis results also quantitatively agree well with the tests under LC conditions.

Finally, the length of non-propagating cracks is quantitatively discussed. The ratios of  $\Delta K$  to  $\Delta K_{th}$  calculated using the above-mentioned model are summarized in Fig. 22 using non-propagating crack length observed in the experiments. Under PC conditions, the ratios of  $\Delta K$  to  $\Delta K_{th}$  were almost 1, as shown in Fig. 22(a). This indicates that the micro crack propagation model estimates non-propagating crack length with considerable accuracy. Under LC conditions, the ratios were 0.8-1.4, as shown in Fig. 22(b), which is also satisfactorily accurate. The test results can be successfully explained using the micro-crack

propagation model, as shown in Figs. 20-22. Therefore, the maximum tangential stress theory is effective for satisfactorily evaluating fretting fatigue strength in stage I as well as in stage II for practical use.

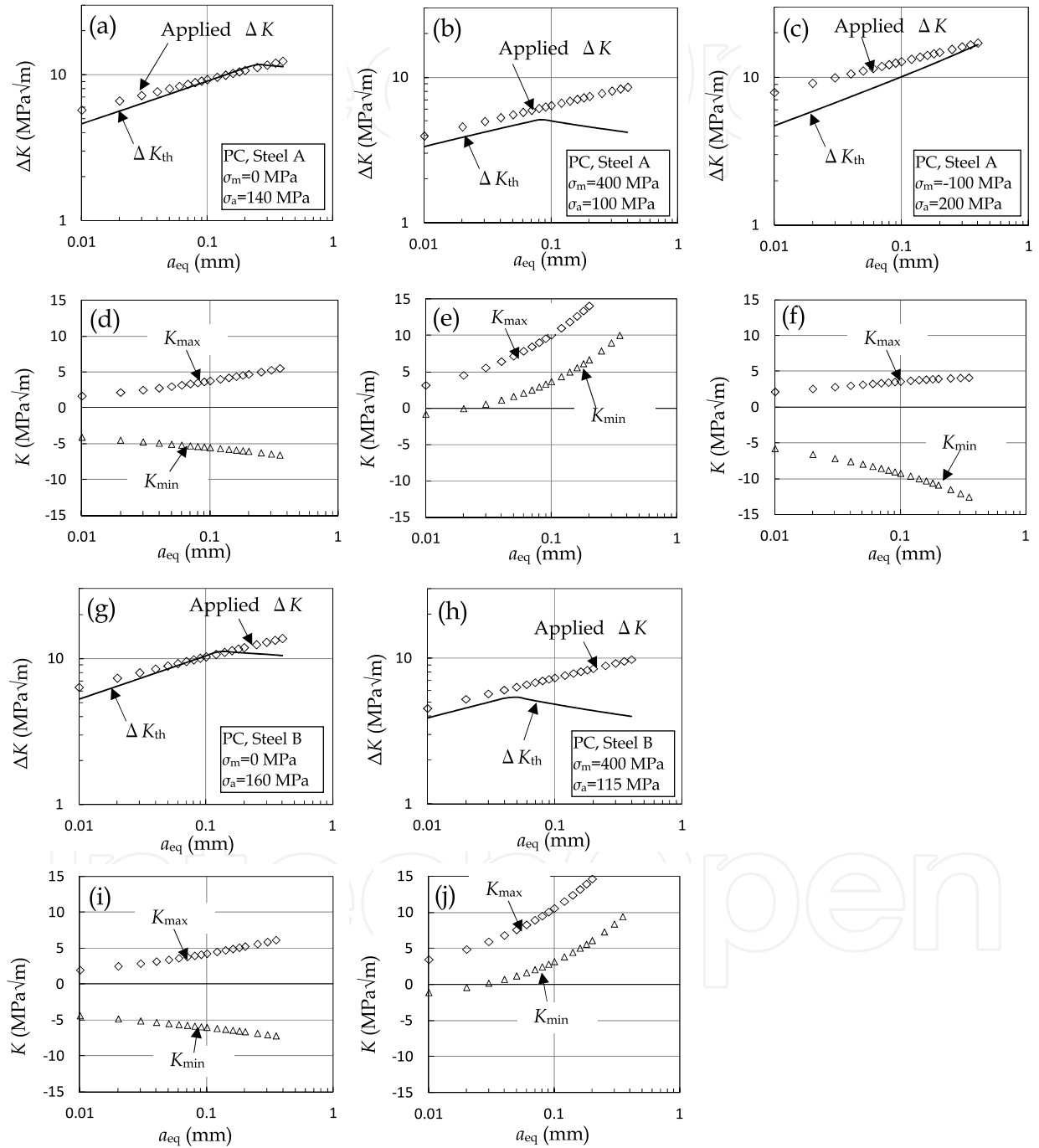


**Figure 20.** Evaluation results on  $\Delta K$ ,  $K_{max}$  and  $K_{min}$  using minimum stress leading to fracture in experiments under PC at  $p=80$  MPa when  $\sigma_m =$  (a)(d) 0 MPa, (b)(e) 400 MPa, (c)(f) -100 MPa for sample A, and  $\sigma_m =$  (g)(i) 0 MPa, (h)(j) 400 MPa for sample B

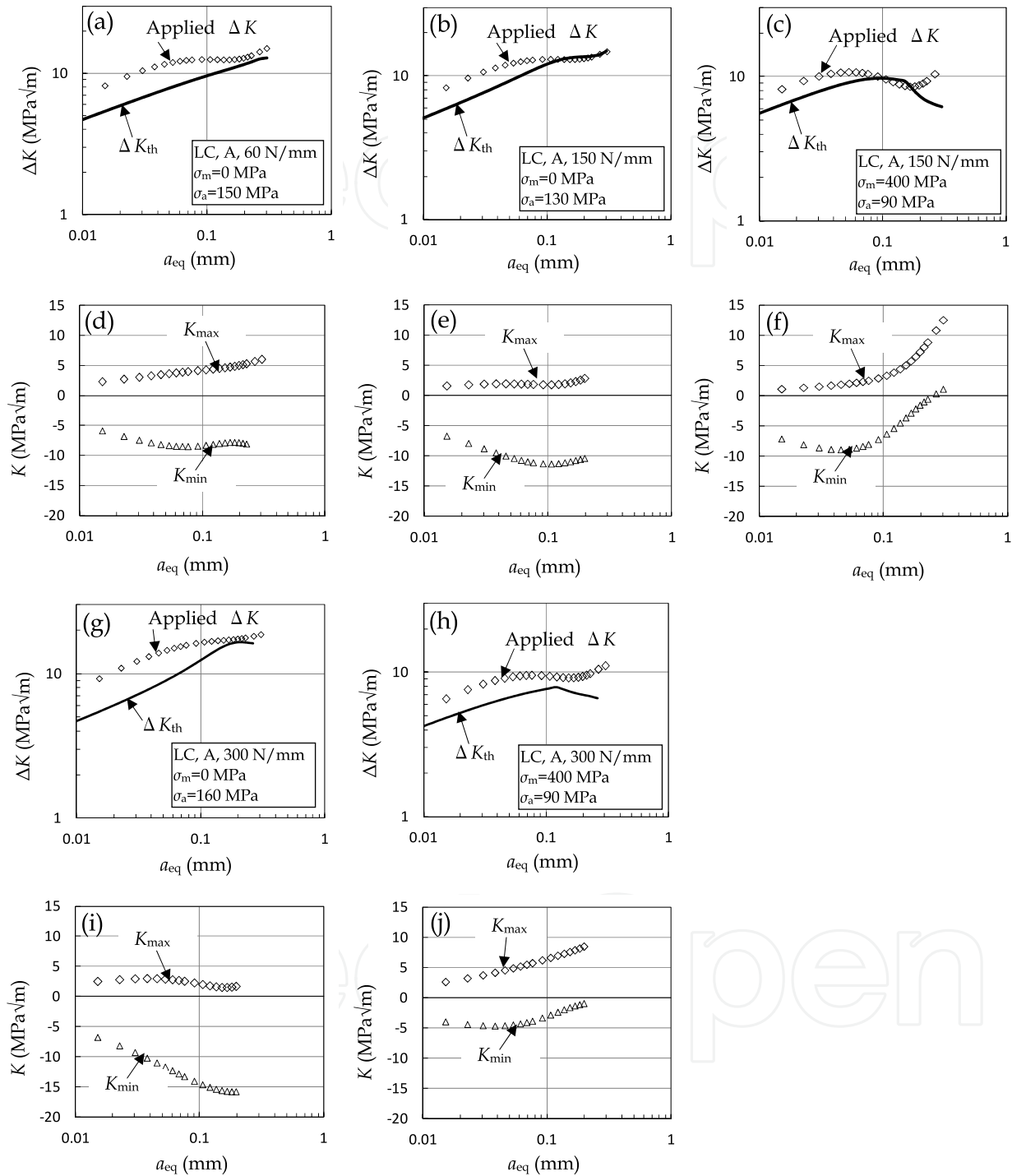


**Figure 21.** Evaluation results on  $\Delta K$ ,  $K_{\max}$  and  $K_{\min}$  using minimum stress leading to fracture in experiments under LC for sample A when (a)(d)  $P=60$  N/mm,  $\sigma_m=0$  MPa, (b)(e)  $P=150$  N/mm,  $\sigma_m=0$  MPa, (c)(f)  $P=150$  N/mm,  $\sigma_m=400$  MPa, (g)(i)  $P=300$  N/mm,  $\sigma_m=0$  MPa, and (h)(j)  $P=300$  N/mm,  $\sigma_m=400$  MPa

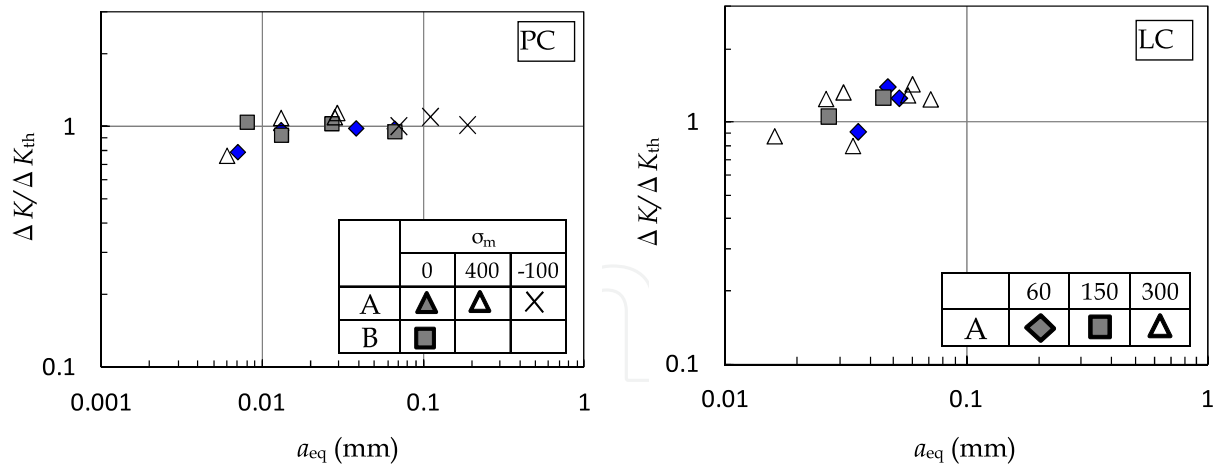


Figure 22. Stress intensity factor ratios of  $\Delta K$  to  $\Delta K_{th}$  of non-propagating cracks for (a) PC and (b) LC

### 5. Conclusion

Fretting fatigue tests were undertaken in LC conditions as well as PC conditions using 12% Cr steel samples with parameters of mean stress, contact pressure, and material strength. The strengths were evaluated quantitatively by applying the micro-crack propagation model under various test conditions considering small crack and mean stress effects on  $\Delta K_{th}$  and mixed modes of tensile and shear  $\Delta K$ . Crack propagation behavior was also examined quantitatively by obtaining non-propagating crack lengths of run-out specimens and  $\Delta K_{th}$  from fretting pre-cracks under several R, including negative mean stress. The results obtained are as follows.

1. Test results concerning the fretting fatigue strength could be successfully explained using the micro-crack propagation model by applying the maximum tangential stress theory in both stages I and II under PC conditions at different mean stresses for samples A and B. Under LC conditions, where high contact pressure arises, it was found that elasto-plastic analysis is necessary for calculating  $\Delta K$  and  $K_{mean}$  considering the actual yield behavior, and the proposed method is effective for expressing test results when  $\sigma_m=0$  and 400 MPa under 60, 150, and 300 N/mm contact pressure for sample A.
2. Cracks were confirmed to propagate in stage II at the angle where the maximum stress intensity factor range  $\Delta K_{\theta_{max}}$  occurred by observing the propagation profile. This model also confirmed the experimental results that the depth of non-propagating cracks decreases as the mean stress and the material strength increase.
3. Under PC at 80-MPa pressure, sample B (the static strength of which was about 40% higher than that of sample A) exhibited 10-25% higher fretting-fatigue strength than sample A. Under LC conditions, the fretting fatigue strength decreased as contact pressure increased and minimized when Hertz's average contact pressure was about 1.5 times 0.2% proof stress. This behavior is explained as two conflicting effects; the increase in  $\Delta K$  accelerates crack propagation and negative large  $K_{mean}$  delays its propagation as the contact pressure increases.

4. Crack propagation data in stage I, such as inclined angles and the boundary depth from stages I to II, were obtained under various test conditions, which is expected to be clarified quantitatively by analyzing mixed mode effects .

## Author details

Kunio Asai  
Hitachi Research Laboratory/Hitachi, Ltd., Japan

## 6. References

- Asai, K. (2010). Fretting fatigue strength of 12% Cr steel under high local contact pressure and its fracture mechanics analysis. *Science Direct, Procedia Engineering*, Vol. 2, pp. 475-484
- ASME section XI appendix A-3000. (2001). Method for  $K_I$  determination, pp. 372-373
- Attia, M. H. (2005). Prediction of fretting fatigue behavior of metals using a fracture mechanics approach with special consideration to the contact problem. *Journal of Tribology*, Vol. 127, pp. 685-6930
- Bold, P. E., Brown, M. W., & Allen, R. J. (1992). A review of fatigue crack growth in steels under mixed mode I and II loading. *Fatigue Fracture Engineering Materials Structure*, Vol. 15, No. 10, pp. 965-977
- Dubourg, M. C., & Lamacq, V. (2000), Stage II crack propagation direction determination under fretting fatigue loading: A new approach in accordance with experimental observations. *ASTM STP 1367*, pp. 436-450
- Edwards, P. R. (1984), Fracture mechanics application to fretting in joints. *Advances in Fracture research*, Pergamon Press, pp. 3813-3836
- El Haddad, M. H., Smith, K. N., & Topper, T. H. (1979). Fatigue crack propagation of short cracks. *Transactions of the ASME*, Vol. 101, pp. 42-46
- Faanes, S. (1995). Inclined cracks in fretting fatigue. *Engineering Fracture Mechanics*, Vol. 52, No. 1, pp. 71-82
- Hannes, D., & Alfredsson, B. (2012). A fracture mechanical life prediction method for rolling contact fatigue based on the asperity point load mechanism. *Engineering Fracture Mechanics*, Vol. 83, pp. 62-74
- Kondo, Y., Sakae, C., Kubota, M., Nagasue, T., & Sato, S. (2004). Fretting fatigue limit as a short crack problem at the edge of contact. *Fatigue Fracture Engineering Materials Structure*, Vol. 27, pp. 361-368
- Lamacq, V., Dubourg, M. C., & Vincent, L. (1996). Crack path prediction under fretting fatigue- A theoretical and experimental approach. *Journal of Tribology*, Vol. 118, pp. 711-720
- Makino, T., Yamamoto, M., & Hirakawa, K. (2000), Fracture mechanics approach to the fretting fatigue strength of axle assemblies. *ASTM STP 1367*, pp. 509-522
- Murakami, Y., & Endo, M. (1986). Effects of hardness and crack geometry on  $\Delta K_{th}$  of small cracks. *Journal of the Society of Materials Science, Japan*, Vol. 35, No. 395, pp. 911-917

- Murakami, Y., Fukuhara, T., & Hamada, S. (2002). Measurement of Mode II threshold stress intensity factor range  $\Delta K_{IIth}$ , *Journal of the Society of Materials Science, Japan*, Vo. 51, No. 8, pp. 918-925
- Mutoh, Y. (1997). Fracture mechanics of fretting fatigue. *Journal of the Society of Materials Science, Japan*, Vol. 46, No. 11, pp. 1233-1241
- Mutoh, Y., & Xu, J.-Q. (2003). Fracture mechanics approach to fretting fatigue and problems to be solved. *Tribology International*, Vol. 36, pp. 99-107
- Nicholas, T., Hutson, A., John, R., & Olson, S. (2003). A fracture mechanics methodology assessment for fretting fatigue. *International Journal of Fatigue*, Vol. 25, pp. 1069-1077
- Pook, L. P. (1985). A failure mechanism map for mixed mode I and II fatigue crack growth thresholds. *International Journal of Fracture*, Vol. 28, pp. 21-23
- Qian, J., & Fatemi, A. (1996). Mixed mode fatigue crack growth: A literature survey. *Engineering Fracture Mechanics*, Vol. 55, No. 6, pp. 969-990.
- Raju, IS. & Newman, JC. (1981). An empirical stress intensity factor equation for the surface crack. *Engineering Fracture Mechanics*, Vol. 15, pp. 185-192
- Tanaka, K. (1974). Fatigue crack propagation from a crack inclined to the cyclic tensile axis. *Engineering Fracture Mechanics*, Vol. 6, No. 3, pp. 493-507
- Usami, S., & Shida, S. (1979). Elastic-plastic analysis of the fatigue limit for a material with small flaws. *Fatigue of engineering materials and structures*, Vol. 1, No. 4, pp. 471-481.
- Zhang, H., & Fatemi, A. (2010). Short fatigue crack growth behavior under mixed-mode loading. *International Journal of Fracture*, Vol. 165, pp. 1-19